

Telecentric Optics for Free-Space Optical Link

Huei Pei Kuo, member IEEE

Robert Walmsley,

Lennie Kiyama,

Michael Tan, member IEEE

and Shih-Yuan Wang, fellow IEEE

HP Labs, Hewlett Packard, 1501 Page Mill Road, Palo Alto, CA 94304

Hueipei.kuo@hp.com, +1-650-857-5407

Abstract -- We describe a telecentric optical system for free-space multichannel optical interconnects. The targeted aggregate data rate is 240Gb/s. We have a unique implementation of telecentric optics and achieved an optical link that is simple, robust and modular. The integrity of the optical link is not significantly degraded with a $>\pm 2$ mm translational misalignment between the transmitter and receiver arrays. With this optical link, we need only a low bandwidth active servo mechanism to compensate for static tilt and possibly low frequency thermally-driven shift between the transmitter and receiver arrays.

I. INTRODUCTION

Optical interconnects have the promise of exceptional bandwidth, low propagation loss, EMI immunity and potentially low power consumption [1]. Free-Space optical link has the added potential of providing a building block for board-to-board (B2B) interconnects and to enable novel interconnect topologies not practical for conventional copper interconnect.

The telecentric lens with unity magnification (1X) has the same magnification at all object/image

distances and is free of field distortion. This makes it attractive for free-space multi-channel optical link. Leyva et al [2] incorporated a light-valve with telecentric optics to compensate for misalignment. Their implementation is complex and did not exploit fully the characteristics of the telecentric lens. The telecentric lenses for commercial applications are typically bulky and expensive. In this paper, we describe a telecentric optical system that can be fabricated using two single-element plano-convex

lenses. We are targeting a free-space B2B optical link with an aggregate bandwidth of 240Gb/s that requires a minimal number of actuators to compensate for B2B misalignments of up to ± 1 mm in-plane offset, ± 5 mm B2B spacing variation and $\pm 4^\circ$ of angular offset (pitch/yaw). The optical link is modular for easy integration into systems.

II. OUR SOLUTION

In this paper we present an optical module for free-space interconnects using a double telecentric lens with unity magnification (1X). We need only two single-element, potentially low-cost, plano-convex lenses to construct the telecentric optics. One half of the telecentric lens is mounted on the board with the emitter array and the other half on the board with the detector array. The lenses are coupled tightly with the emitter and the detector arrays respectively.

A schematic of the multichannel optical link with telecentric optics is depicted in Figure 1 for a B2B spacing of ~50 mm.

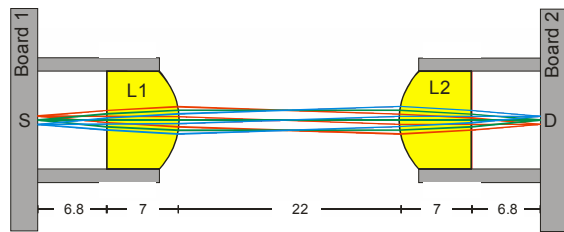


Figure 1. Telecentric Optics for B2B optical interconnects. The distance between board 1 (B1) and board 2 (B2) is ~50mm. Two identical single-component plano-convex lenses, L1 and L2, forms the telecentric lens to focus the emission from the emitter array, S, on B1 onto the matching detector array, D, on B2 with a unity magnification (1X). L1 is mounted on B1 and L2 is mounted on B2. The distances between the optical elements are shown in mm. An identical set of telecentric optics (not shown) focuses emission from the emitter array on B2 to the detector array on B1 to complete the bi-directional link between the boards.

We use Zemax® optics simulation program to optimize the optics and to help estimate cost. Figures 2 and 3 depict the predicted dimensions and shapes of the images, on board 2, formed by the telecentric optics of an array of emitters on board 1. The simulation shows that the telecentric optics focuses the emission for individual emitters into a dimensions of $\leq 15 \mu\text{m}$. Emission from a vertical-cavity-surface-emission-laser (VCSEL) emitter with an emission area of $\sim 5 \mu\text{m}$ in diameter would be focused into an image with a linear dimension $\leq 20 \mu\text{m}$. Equally importantly, the field distortion of the telecentric optics is predicted to be $< 5 \mu\text{m}$ for all the VCSELs in the array. This is more than adequate for high-speed GaAs PIN detectors with a diameter of $\sim 50 \mu\text{m}$. Simulations indicate that our optics can accommodate arrays of $> 1 \text{ mm} \times 1 \text{ mm}$. Figure 3 shows the characteristics of the focused emission when the lens L2 and the detector array assembly is shifted by 1 mm from lens L1 and the emitter array. The emission is still focused to an area with linear dimensions $\leq 20 \mu\text{m}$. The centroids of the images of the emitters and the corresponding detectors are misaligned by $\leq 5 \mu\text{m}$, still adequate for our application. The emission semi-angle of a typical VCSEL is $\sim 10^\circ$. The emission is focused into an area with linear dimensions of $\sim 25 \mu\text{m}$ without the use of angular limiting aperture. This is still quite adequate.

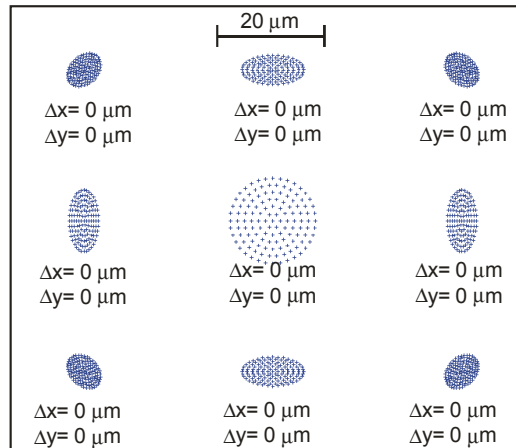


Fig. 2. Spot diagrams of the images on the detector board of the emission from a 3x3 emitter array. The spacing between the emitters and the detectors are $375 \mu\text{m} \times 375 \mu\text{m}$. The emitter and the detector arrays are aligned with the telecentric optics and the semi angle of emission is set to 5° . The spacing between the emitter and the detector arrays is 50 mm. The emission from the individual emitters is focused into areas with linear dimensions of $< 20 \mu\text{m}$. The magnitudes of the field distortion at the plane of the detector board are noted below the respective spot diagrams. There is no field distortion with our implementation of the double telecentric lens with unity magnification. The emitter array is perfectly imaged onto the detector array.

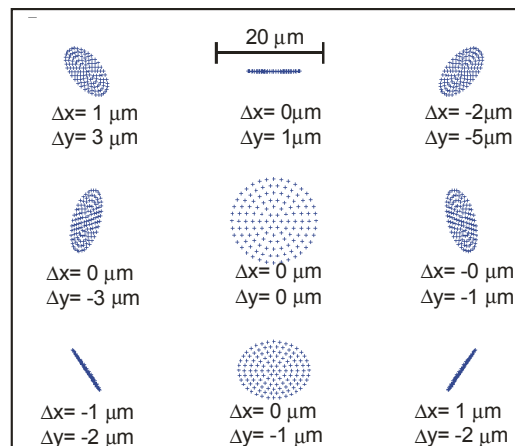


Fig. 3. Spot diagrams of the images on the detector board of the emission from the same 3x3 emitter array in Fig. 2. Lens L2 and the detector array are shifted in y-direction by 1 mm from L1 and the emitter array. The maximum deviation of the centroids of all the emitters is $\leq 5 \mu\text{m}$ from their respective detectors. The emission from the individual emitters is still focused into areas with linear dimensions of $< 20 \mu\text{m}$.

If the boards are tilted with respect to each other, the focused emission is offset globally relative to the detector array. For a 1° tilt, the offset is computed to be ~200 μm. This is a static offset and can be compensated by realigning the lenses using an active servo mechanism. An uncorrectable offset of < 5 μm remains, after the global offset is compensated for. The dimensions of the focused emission remain at < 20 μm. Both the focused beam and the residual offset are more than adequate for our application.

This implementation makes our optics robust and tolerant to misalignment between the boards. A translational misalignment of > ±1 mm between the transmitter and detector arrays does not degrade the integrity of the link appreciably. This robustness allows us to greatly simplify the servo mechanism of the optics: we need only two single-axis actuators to compensate for tilt misalignment and one actuator for the axial rotation misalignment between the transmitter and the detector arrays.

We have designed and constructed optical benches to characterize the optical and mechanical properties of the telecentric optics. Figure 4 and 5 show photographs of the optical bench for characterizing the imaging properties of the telecentric optics. A 1x4 array of VCSEL is used as the emitters. The spacing between the adjacent emitters is 250 μm. The CCD sensor of an ISG LW5-5-1934 monochrome camera is used as the imager. The pixel size of sensor is 2.2 μm x 2.2 μm. This provides sufficient resolution for recording the image on the detector plane.

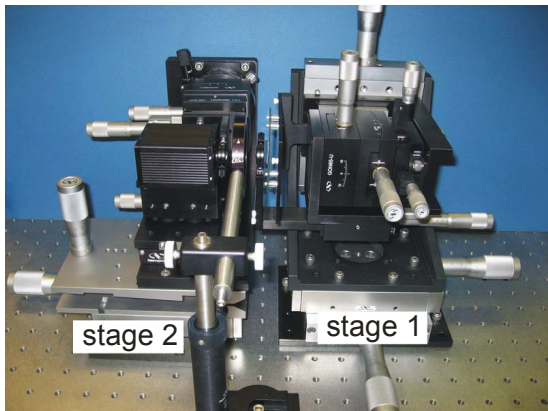


Fig. 4. Optical bench for measuring the imaging properties of the telecentric optical link. There are two independent stages. Details of the emitters, detectors and the optics are depicted and described in Fig. 5.

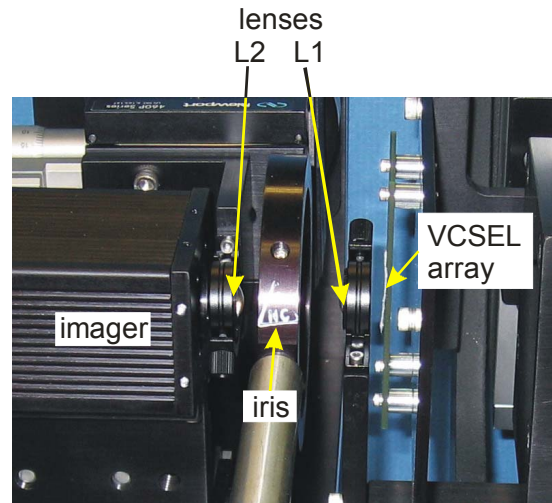


Fig. 5. Close-up view of the central section of the optical bench shown in Fig. 3. A 1x4 VCSEL array and a plano-convex lens, L1, is mounted on stage 1. The CCD imager and L2 are mounted on stage 2. Both stages are equipped with sufficient number of micrometer controls to allow adjustment of tilt, rotation, spacing and lateral offsets between the emitter array, detector array and the lenses. This allows us to do a complete emulation of the physical environment in real computer systems where the optical links are to be implemented, such as adjacent blades of HP Blade Servers. An optional iris can be inserted at the common focal plane of lenses L1 and L2 to limit the emission angle.

Figure 6 shows focused images of the emission from the 1x4 VCSEL array at an emission power of 1 mW and at emission semi angle of 5° and 15°. The intensity profile of the image of the VCSEL, second from the top and operating at 1000 μW at 15° semi angle is magnified and shown in Fig. 7.

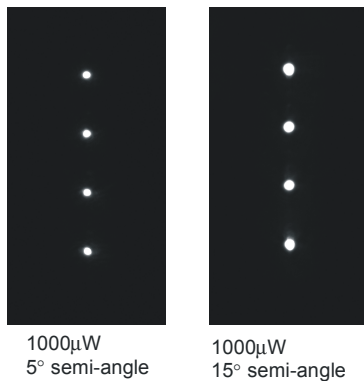


Figure 6. Focused VCSEL emission. The distance between the adjacent spots is 250 μm . The image of the VCSEL, second from the top operating at 1000 μW and 15° semi angle is magnified and shown in Fig. 7 below.

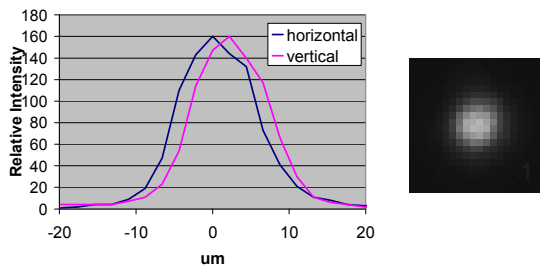
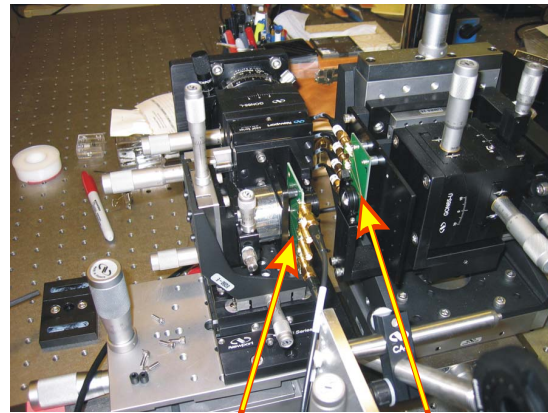


Figure 7. Magnified spot diagrams at 1000 μW and 15° semi angle. The full width at 10% maximum is approximately 20 μm .

To measure the coupling of the emission from the VCSEL to a detector array, the imager depicted in Fig. 6 & 7 is replaced by a 1x4 array of GaAs PIN detectors. The modified configuration of the optical bench is shown in Fig. 8. The characteristics of the link are investigated at DC and 2Gbps. The VCSEL array is driven with a 200Hz square wave for DC characterization. The coupled signals on the detector array are shown in Fig. 9. About 90% of the emitted power from the VCSEL is transmitted through the optical system. Most of the loss is from the reflections at the lens surfaces. An improved efficiency can be achieved with optimized antireflective coating on the lenses. The measured cross talk between adjacent channels is $< -30\text{db}$.



1x4 Detector array 1x4 VCSEL array

Fig. 8. Optical bench for measuring the coupling of the emission from the VCSEL array to the detector array.

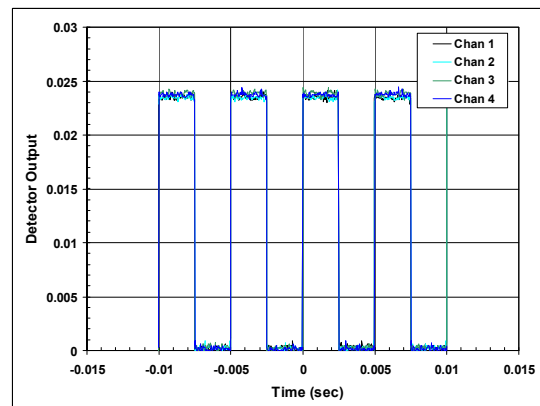


Fig. 9. Detector signal when the optics is properly aligned and focused. ~90% of the emitted power from the VCSEL is transmitted through the optical system. Most of the loss is from the reflections at the lens surfaces. An improved efficiency can be achieved with optimized antireflective coating on the lenses.

The peak power output of the detectors is measured as a function of misalignment between the emitter and the detector arrays. To emulate the translational misalignment between the adjacent boards in a Blade Server Chassis, lens L1 and the VCSEL array are translated together relative to the L2 and detector array. The peak output as a function of the misalignment is shown in Fig. 10. It shows that the output power is not significantly affected with a displacement of up to $\pm 2\text{ mm}$.

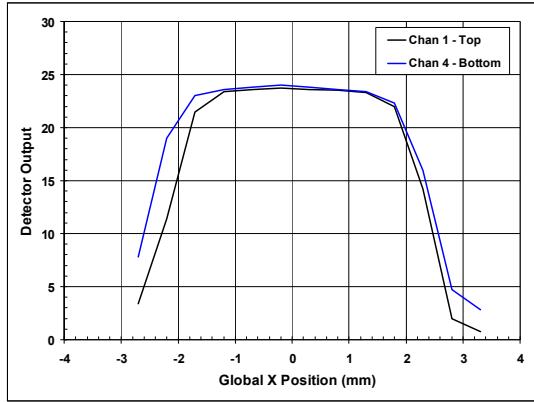


Fig. 10. Detector peak-to-peak output vs lateral displacement between the VCSEL array and the detector array. Lens L1 and the VCSEL array are shifted together relative to lens L2 and the detector array. The output stays relatively constant with a ± 1 mm displacement.

Figure 11 depicts the effect of the VCSEL array and lens L1 is tilted relative to the detector array and lens L2 in the same fashion described above for lateral displacement. It shows that the tilt angle needs to be kept to be less than $\sim 0.1^\circ$ to avoid degrading of the optical power at the detectors. This is in agreement with the design of the telecentric optics. In the configuration shown in Fig. 3, a 0.1° tilt produces a shift of $\sim 20 \mu\text{m}$ of the image of the VCSEL in the plane of the detector array and the image of the VCSEL will start to miss the active area of the detectors.

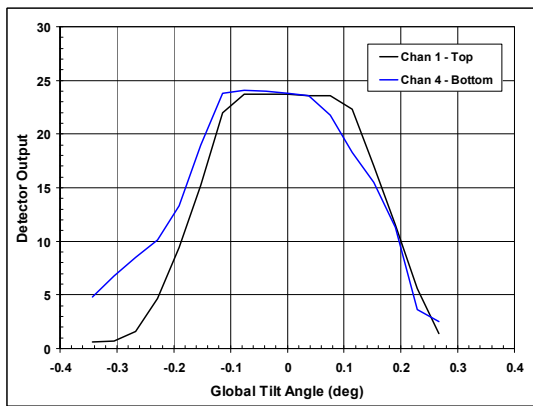


Fig. 11. Detector peak-to-peak output vs tilt angle.

We measured the operation of the optical link at 2Gbps. Maximum operational bit rate on our testbed is currently limited by the electronics. Figure 12

shows an eye diagram of the 2Gbps operation.

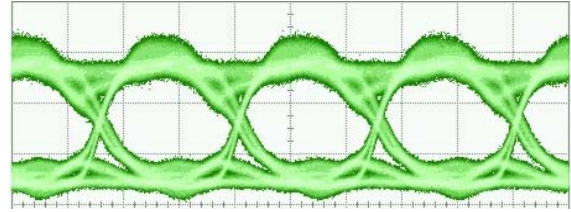


Fig. 12. Eye diagram showing the operation of the telecentric free-space optical link at 2GHz. Time scale (horizontal) is 200ps/div

We also measured the dynamic offset between the boards caused by vibrations of an HP production Blades Server, Proliant BL480C with a set-up shown in Fig. 13. The results are shown in Fig. 14. The major sources of the vibration are the cooling fans and the disk drives. The measured data indicate that the dynamic displacement caused by vibrations is less than $< \pm 1 \mu\text{m}$. The vibration has the typical $1/f$ dependency on frequency with spikes that coincide with the rotational frequencies of the motors of the cooling fans and disc drives. This magnitude of displacement is well within tolerance to maintain a good optical link as shown in Fig. 10 and 11.

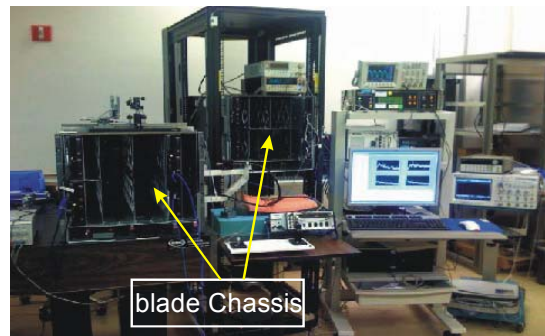


Fig. 13. Set-up for measuring the mechanical vibration characteristic on HP Blade System. One chassis can accommodate up to 8 blade servers.

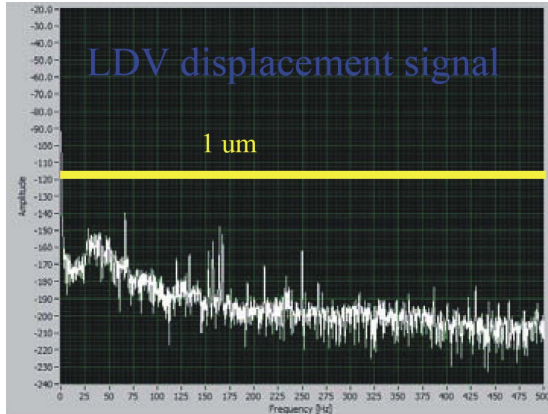


Fig. 14. The magnitude of vibration as a function of frequency of an HP production Blades Server, Proliant BL480C. Total displacement of vibration is under 1um. The dominant frequencies of the vibration are at ~50Hz from the cooling fans and at ~200 Hz from the disc drive motors.

We measured the displacements of the HP production Blades Servers, Proliant BL480C, with respect to each other under repeated removal and insertion of the boards. Experimental data indicate that repeated removal and insertion of the boards produce a static non-repeatable in-plane offset of $< \pm 250 \mu\text{m}$ between the boards along the insertion (horizontal) axis and $< \pm 50 \mu\text{m}$ in the vertical axis. The results are shown in Figure 15. We also measured the static offset and initial turn-on drift of the blades. The results are shown in Figure 16.

Unplug/Plug Blade -1/2 Removal

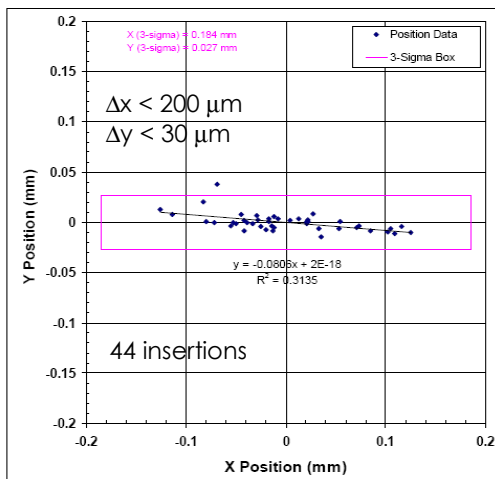


Fig. 15. In-plane offset of an HP production Blades Servers, Proliant BL480C under repeated insertion and removal of the boards.

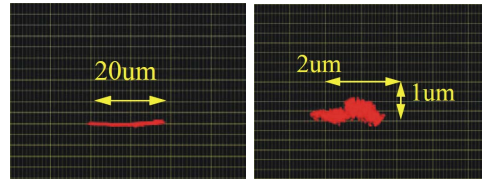


Fig. 16. Scatter plots of the position of blades of an HP production Blades Servers, Proliant BL480C. The left panel shows the turn-on drift and the right panel shows the residual random walk when the blades are turned off. Horizontal axis shows the drift in the horizontal direction, which is also the direction of insertion.

III. Summary

We have designed a telecentric optical link for free-space optical interconnect. We have also built an optical benches and measured the optical and mechanical properties of the system. The displacement between the boards caused by vibration is small and does not require active compensation. Only the compensation for initial static misalignment and possibly low frequency thermally-driven shift appear to be required. The telecentric optics and the unique mounting configuration make our optical link robust and tolerant to mechanical misalignment and vibration. We anticipate the optical link could be made into a module with small foot print and could be manufactured at low cost and integrated easily into the design of computer systems at various stages of development.

References

1. Sadik Esener and Phlippe Marchand, Materials Science in Semiconductor Processing, 3, 5-6, pp 433-435, 2000
2. Leyva, DG et.al. Applied Optic 45, 1, pp 63-75, 2006.